Electron-Lattice interaction under high pressure by single-crystal diffraction study

Pressure-induced structure change
due to electron-spin-lattice interaction under extreme condition

charge displopornation　charge transfer　density of state change
orbital rearrangement　Jahn-Teller transition　high-low spin transition
spin-Peierls transition　Motto transition　magneto distortion　etc.

Experiments

1. Possible spin cross over and electron configuration change of Mn_2O_3 detected by X-ray emission spectrum analysis.
2. Difference in Jahn-Teller distortion of Fe_2TiO_4 ulvöspinel at high pressure and at low temperature by MEM .
3. Anisotropy of Electric conduction in $FeTiO_3$ with increasing pressure.

collaborators

Akira Yoshiasa Department of Geoscience Kumamoto University
Osamu Ohtaka Department of Earth and Space Science Osaka University
Takaya Nagai Department of Geology Science Hokkaido University
Taku Okada Institute of Solid State Physics University of Tokyo
Yuki Nakamoto Center for quantum Science and Technology
under extreme conditions Osaka University

Ho-Kwang Mao Carnegie Institute of Washington
Russel Hemley Carnegie Institute of Washington
Wendy Mao Stanford University

Graduate Students
Department of Earth and Space Science Osaka University
Takanori Hattori Taku Tsuchiya Jun Tsuchiya
Hironori Nomori Yutaka Komatsu Tetsuro Mine
Hiroaki Uchida Hiroaki Sugita Yukiko Asogawa
and many others

Octahedral distortion by Jahn-Teller effect

Strong CFSE effect in the cubic - to- tetragonal transition $3d^4$ (Mn^{3+}, Cr^{4+}, Fe^{4+})
$3d^9$ (Cu^{2+})

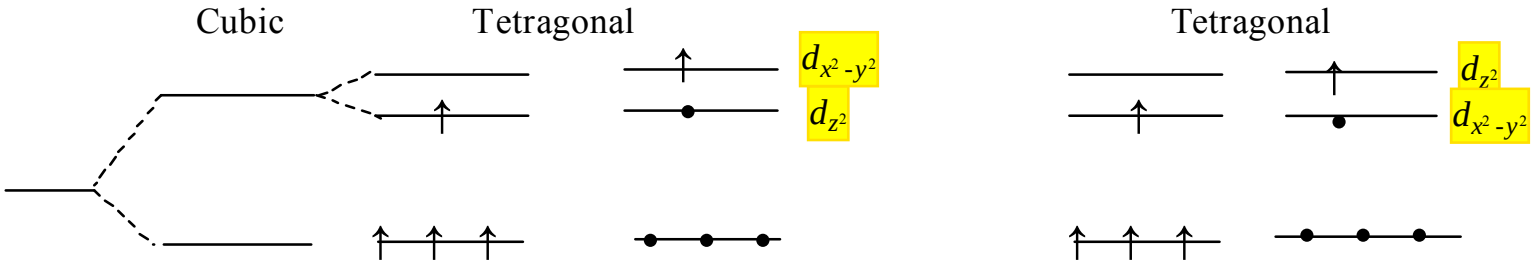

structure	elongation octahedra	flattened octahedra
	c/a>1	c/a<1

Week CFSE effect in the cubic - to- tetragonal transition $3d^2$ (Ti^{2+}, V^{3+}, Cr^{4+})
$3d^7$ (Co^{2+}, Ni^{3+})

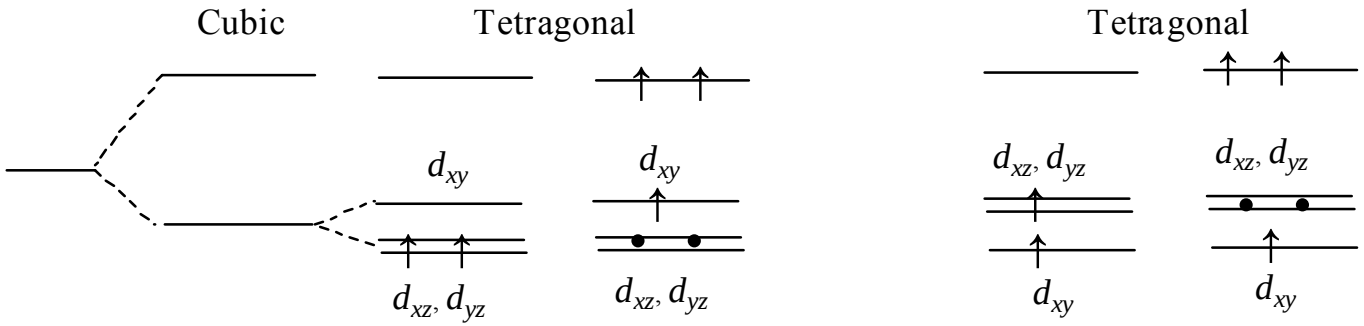

structure	elongation octahedra	flattened octahedra
	c/a>1	c/a<1

X-ray emission spectra of transition elements

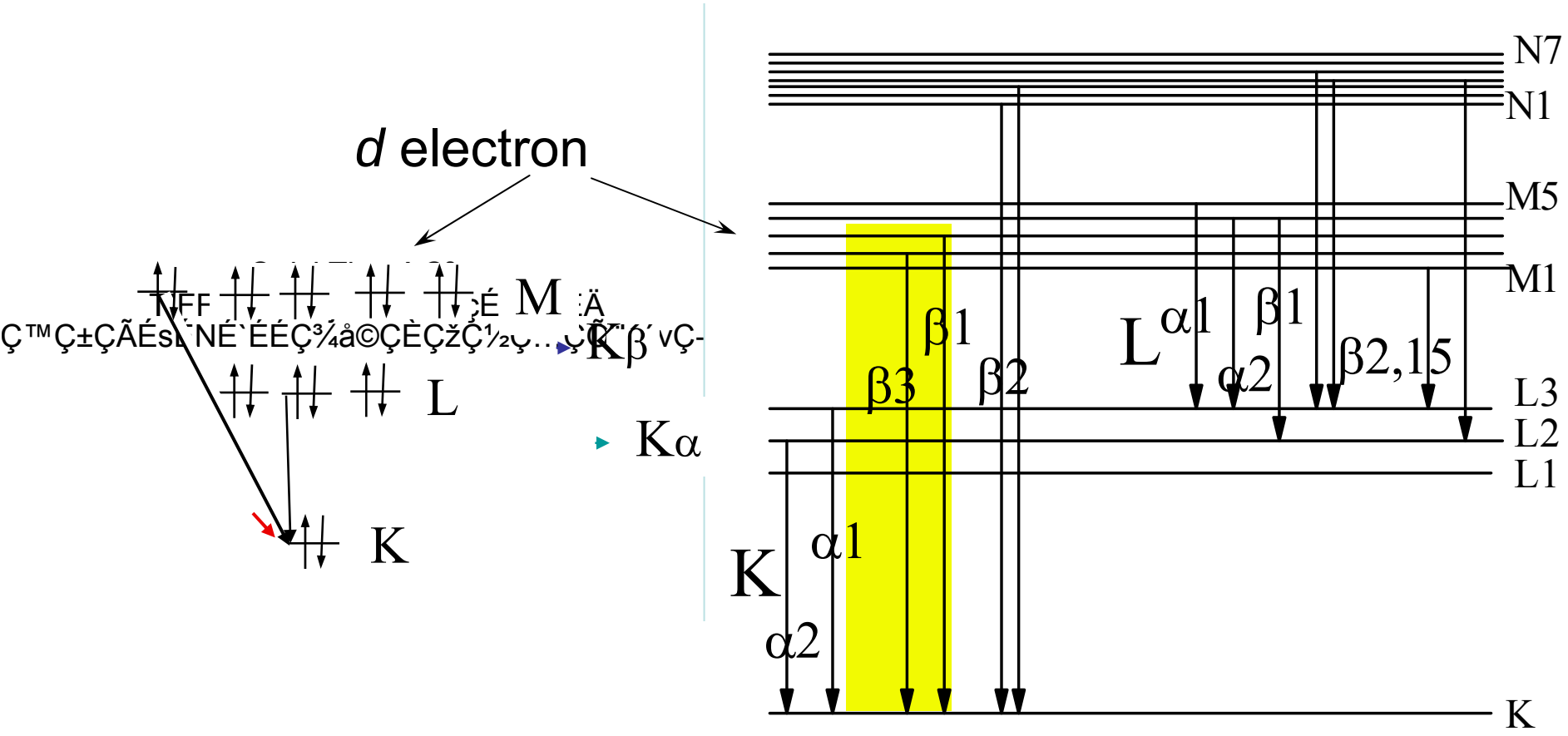

Energy diagram of $3d^4$

Tanabe-Sugano Diagram

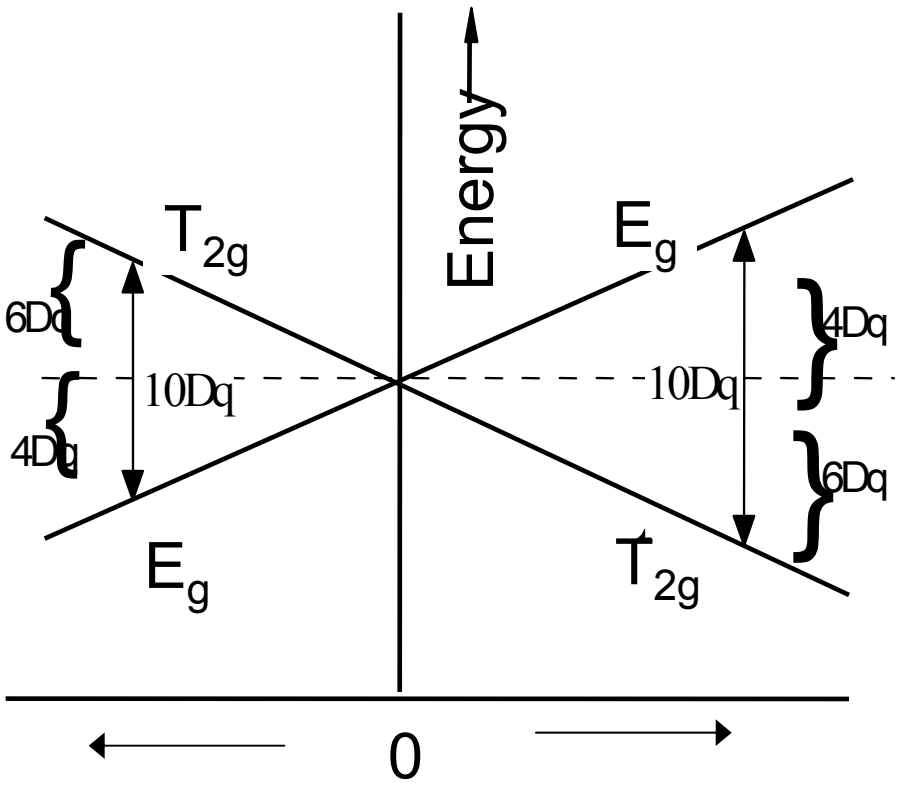

QuickTimeý Ç²
TIFFÀìLZWÀj êLíÉÉvÊçÉOÉâÉÂ
Ç™Ç±ÇÃësÉNÉ´ÉÉÇ¾à©ÇÉÇ±Ç½Ç…ÇÒÏKóvÇ-Ç□ÀB

d^4, d^9 in Oh
d^1, d^6 in Td

d^4, d^9 in Td
d^1, d^6 in Oh

d^1 : Ti^{3+} V^{4+} Cr^{5+}
d^4 : Cr^{2+} Mn^{4+} Fe^{5+}
d^6 : Fe^{2+} Co^{3+} Ni^{4+}
d^9 : Cu^{2+}

D/B

Mn_2O_3 high-pressure transition

at ambient temperature

QuickTimeý Ç²
TIFFÅiLZWÅj êLí£ÉvÉçÉOÉâÉÄ
Ç™Ç±ÇÃÉsÉNÉ`ÉÉÇ¾å©ÇÈÇžÇ½Ç…ÇÕïKóvÇ-Ç

Three polymorphs

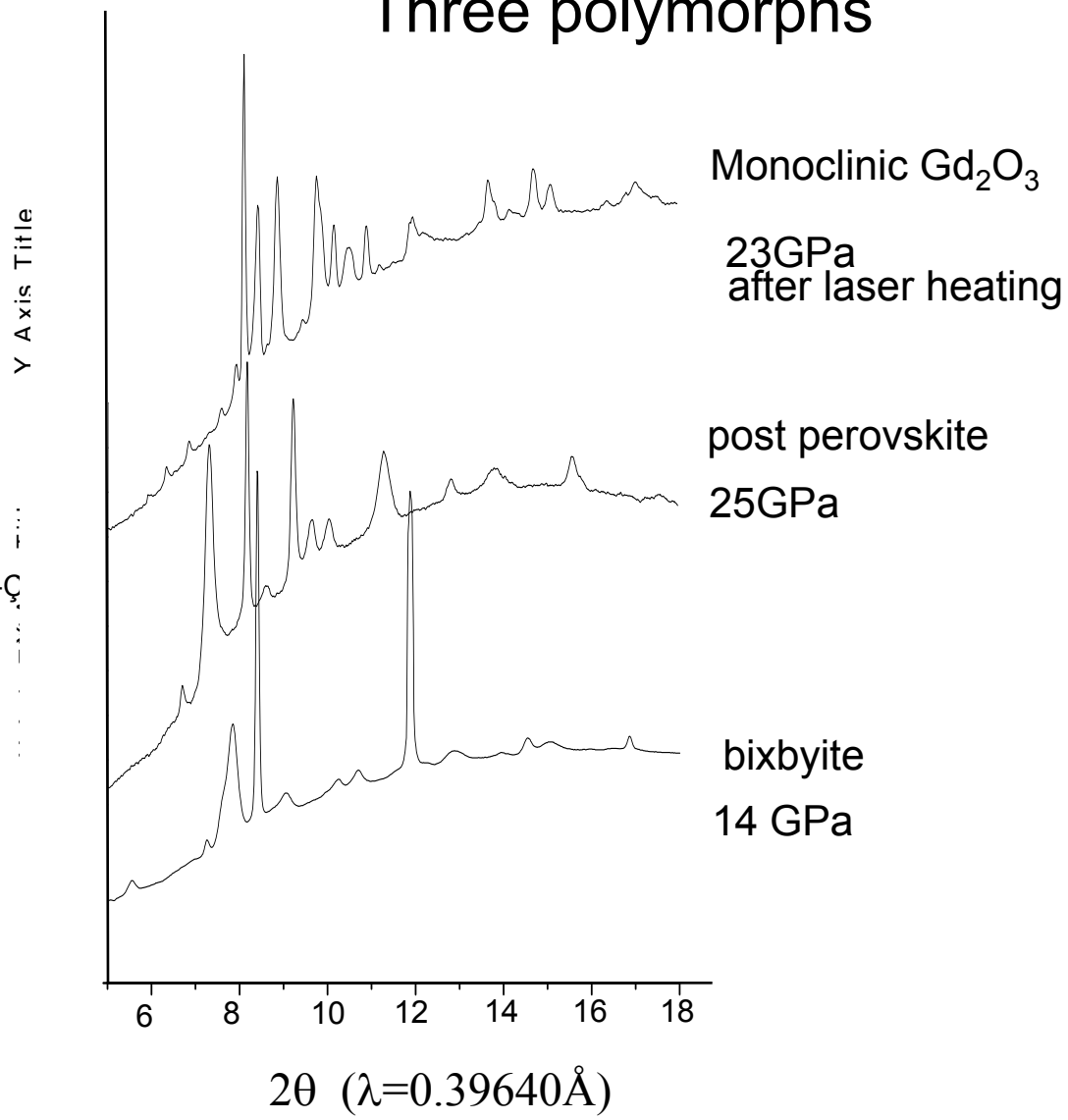

Selected M_2O_3 structure type and r_M/r_O ion radius ratio

	corundum	structure	*R3c*	*Z*=6
	mineral name	a (Å)	c (Å)	Z.	$r_{(M)}/r_{(O)}$
α-Al_2O_3	corundum	4.7628	13.0032	13	0.489
Ti_2O_3	----------	5.148	13.636	22	0.587
V_2O_3	karelianie	5.105	14.449	23	0.565
Cr_2O_3	eskolite	4.957	13.584	24	0.547
α-Fe_2O_3	hematite	5.035	13.72	26	0.500

	rare earth C-type structure		*Ia*$\bar{3}$	**Z=16**
	mineral name	a (Å)	Z.	$r_{(M)}/r_{(O)}$
Sc_2O_3		9.845	21	0.643
* Mn_2O_3	bixbyite	9.4088	25	0.521
Y_2O_3	----------	10.604	39	0.753
In_2O_3	----------	10.118	49	0.681
La_2O_3	----------	11.38	57	0.849
Pr_2O_3	----------	11.136	59	0.819
Nd_2O_3	----------	11.048	60	0.814
Sm_2O_3	----------	10.990	62	0.796
Eu_2O_3	----------	10.840	63	0.788
Gd_2O_3	----------	10.798	64	0.781
Dy_2O_3	----------	10.667	66	0.762
Er_2O_3	----------	10.866	68	0.746
Tm_2O_3	----------	10.604	69	0.739
Yb_2O	----------	10.439	70	0.730

*bearing a little amount of Fe_2O_3 component.

Z denotes the atomic number.

Bixbyite structure

QuickTimeý Ç²
TIFFÂiLZWÀj êLíŁÉvÉçÉOÉâÉÄ
Ç™Ç±ÇÃÉsÉNÉ`ÉÉÇ¾å©ÇÈÇžÇ½Ç…ÇÕïKóvÇ-Ç□ÅB

Mn1 Mn2

SG: *Ia*$\bar{3}$ z=16

a = b = c = 9.4142Å

M1 8a $\bar{3}$ 6-fold

M2 24d .2. 6-fold

Mn_2O_3 of post -perovskite phase at 32.5GPa

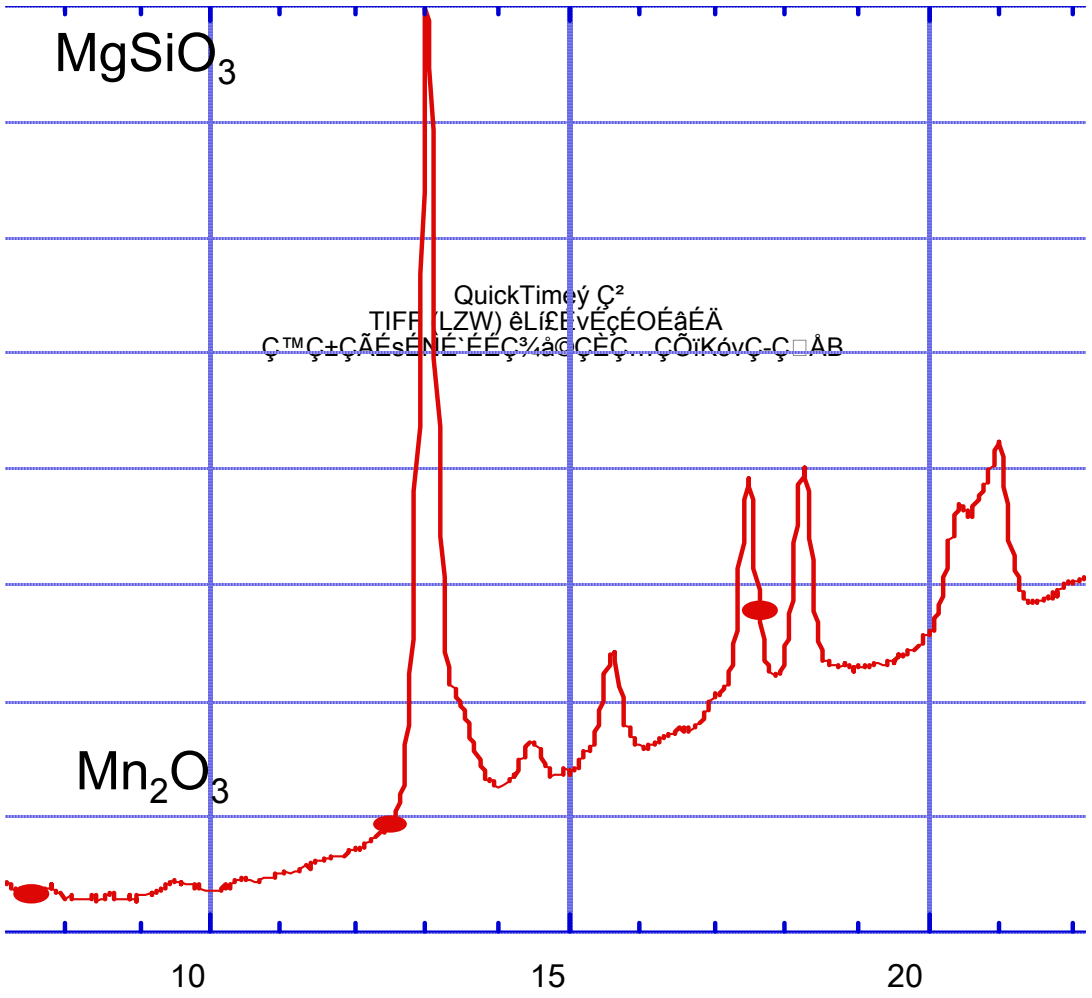

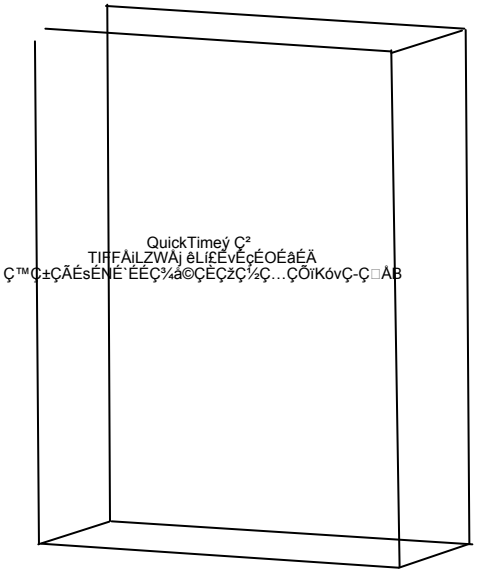

[010]

[101]

[010]

SG: *Cmcm* z = 4

a=2.7498 b=9.0189 c=6.7711Å

Mn1 4c m2m 6-fold

Mn2 4a 2/m 8-fold

Mn_2O_3 of monoclinic Gd_2O_3 type phase at 23 GPa

after laser heating

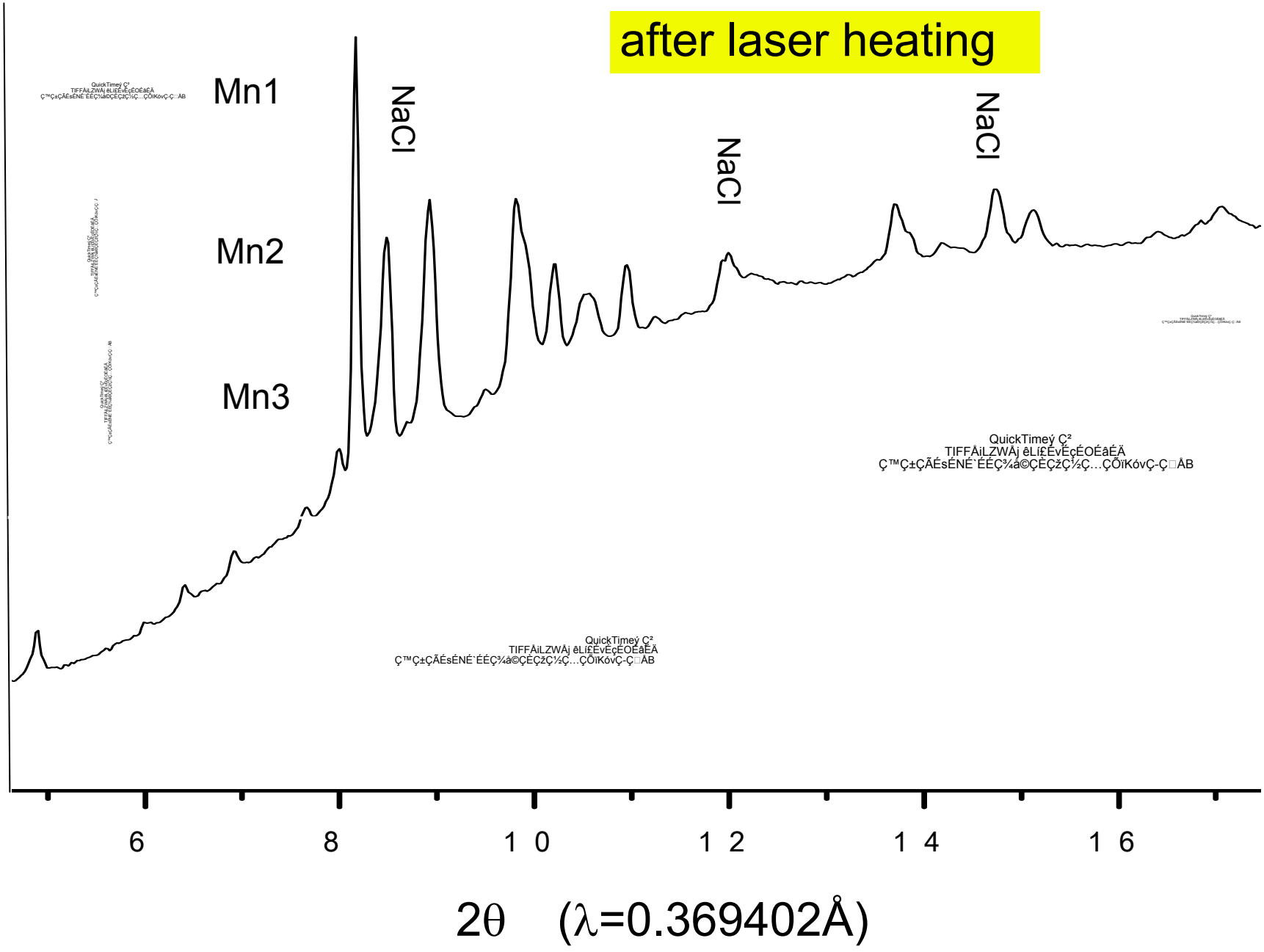

X-ray Emission Spectroscopy set up at APS 16ID-D

QuickTimeý Ç²
TIFFÀiLZWÅj êLí£ÉvÉçÉOÉâÉÄ
Ç™Ç±ÇÃÉsÉNÉ`ÉÉÇ¾â©ÇÈÇžÇ½Ç…ÇÕïKóvÇ-Ç□ÅI

detection of spin state and charge displopornation

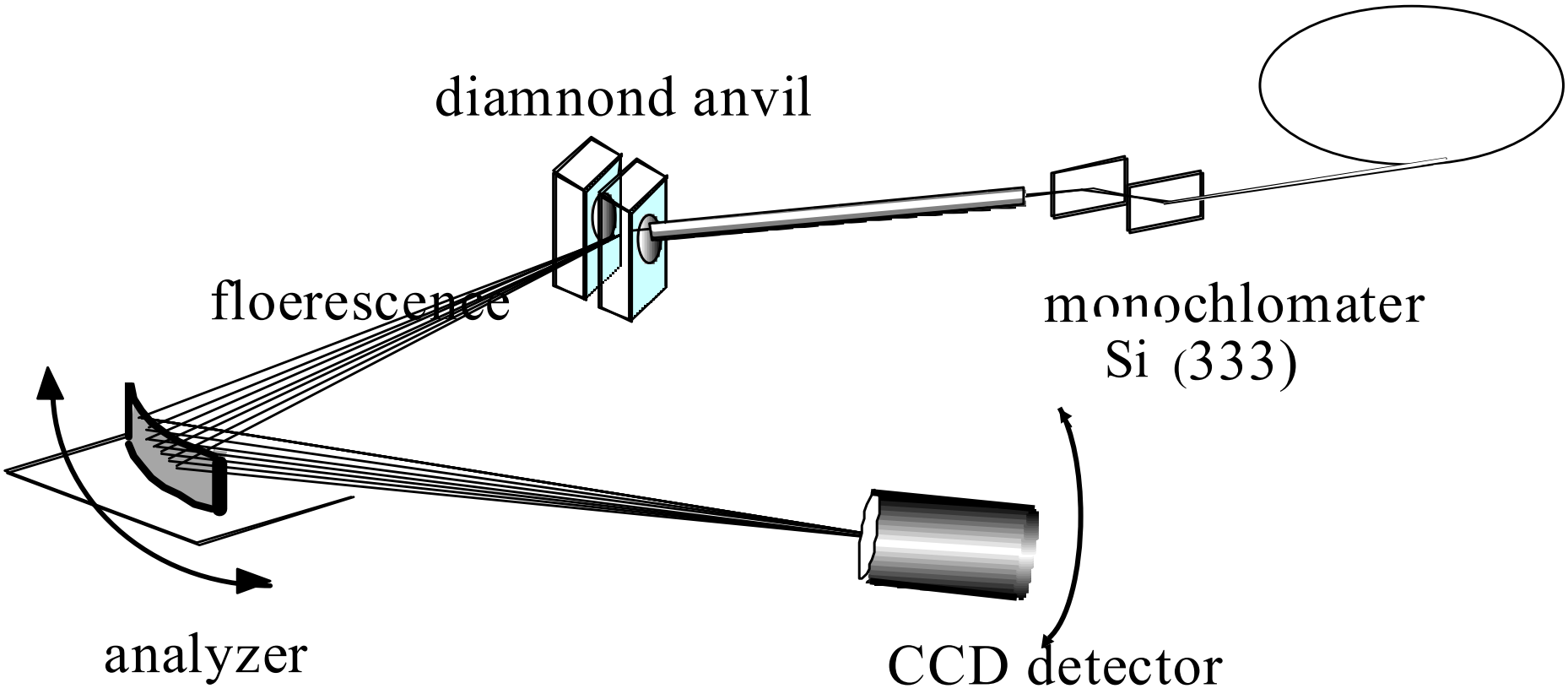

X-ray emission spectra of various Mn oxides

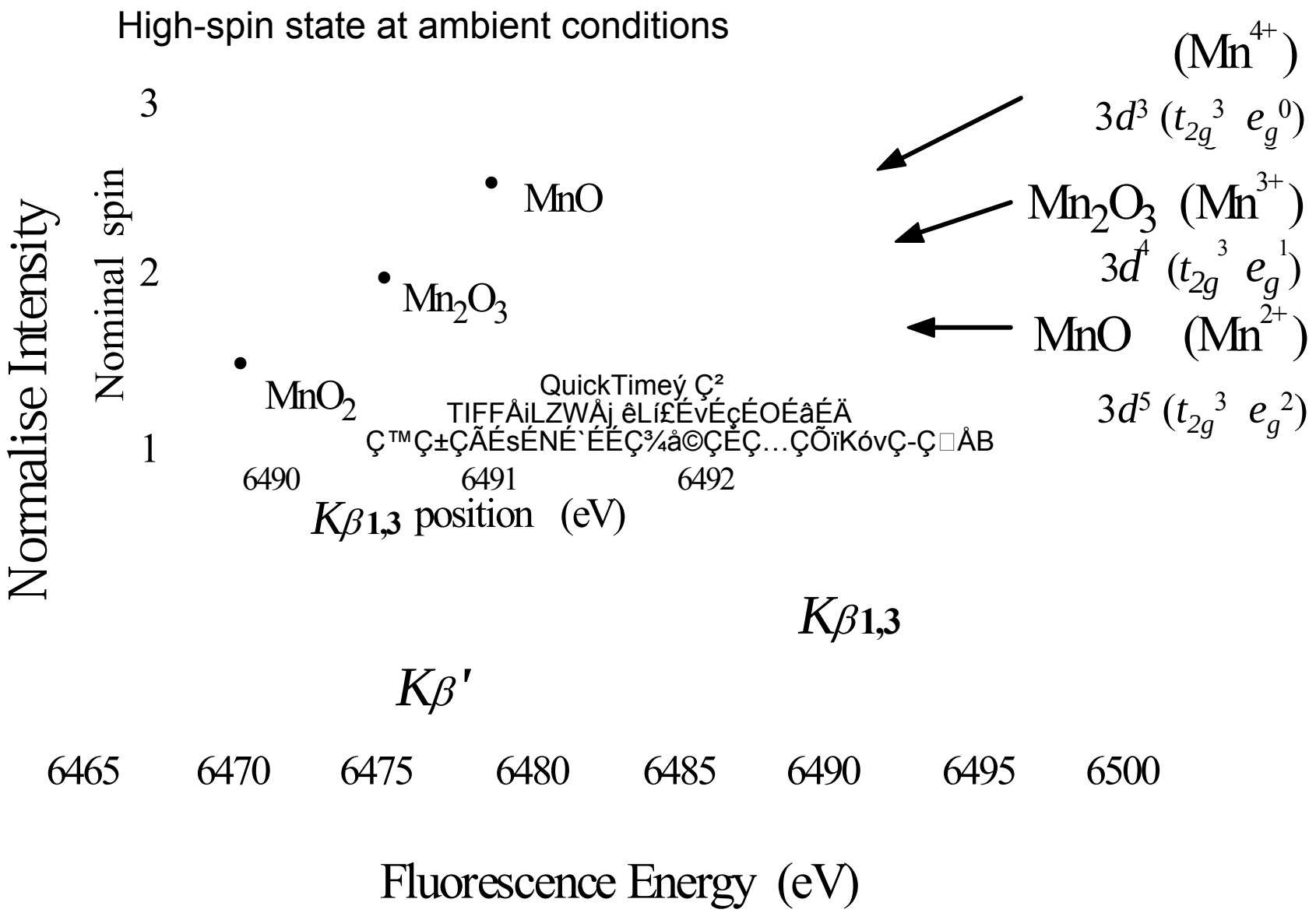

X-ray emission spectrum of Mn_2O_3

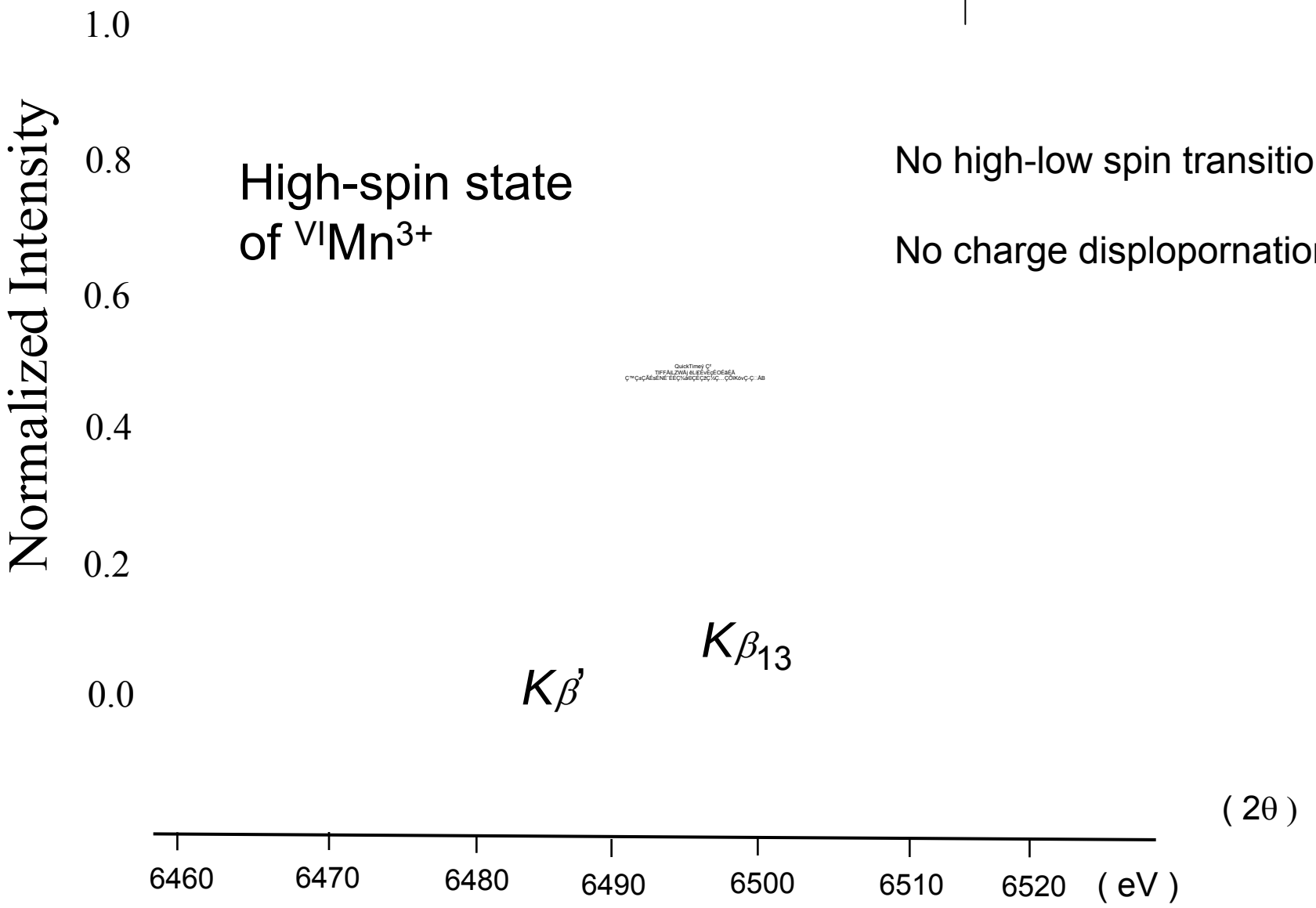

No high-low spin transition

No charge displopornation.

Strong Jahn-Teller effect on the tetrahedral site by single-crystal diffraction study under low-temperature and high-pressure

Sample :

Fe_2TiO_4 ulvöspinel

Inverse spinel structure $(Fe^{2+})[Fe^{2+},Ti^{4+}]O_4$

Fd3m $z=8$ $a=8.5297$Å

antiferromagnetic

Jahn-Teller cation in the tetragonal spinels

Sample	type	stability	J-T ion	configuration	c/a
$MgTi_2O_4$	Inverse	T<260K	Ti^{3+} ($3d^1$)	$\varepsilon(d_{x^2-y^2})$	0.996
$^{A}(Ti^{3+})^{B}[Mg^{2+},Ti^{3+}]O_4$					
Fe_2TiO_4	Inverse	T<142K	Fe^{2+} ($3d^6$)	$\varepsilon(d_{z^2})$	1.05
$^{A}(Fe^{2+})^{B}[Fe^{2+},Ti^{3+}]O_4$		7<P<11GPa		$\varepsilon(d_{x^2-y^2})$	0.998
$CuCr_2O_4$	Normal	T<893K	Cu^{2+} ($3d^9$)	$\varepsilon(d_{x^2-y^2})$	0.915
$^{A}(Cu^{2+})^{B}[Cr^{3+}]_2O_4$					
$NiCr_2O_4$	Normal	T<299K	Ni^{2+} ($3d^8$)	$\varepsilon(d_{z^2})$	1.032
$^{A}(Ni^{2+})^{B}[Cr^{3+}]_2O_4$					
$NiMn_2O_4$	Normal	T<2303K	Ni^{2+} ($3d^8$)	$\varepsilon(d_{z^2})$	0.907
$^{A}(Ni^{2+})^{B}[Mn^{3+}]_2O_4$		0<P<12GPa	Mn^{3+} ($3d^4$)	$\varepsilon(d_{z^2})$	
$CoFe_2O_4$	Inverse	******	Fe^{2+} ($3d^6$)	$\varepsilon(d_{z^2})$	1.17
$^{A}(Ti^{3+})^{B}[Mg^{2+},Ti^{3+}]O_4$					

High pressure experiment

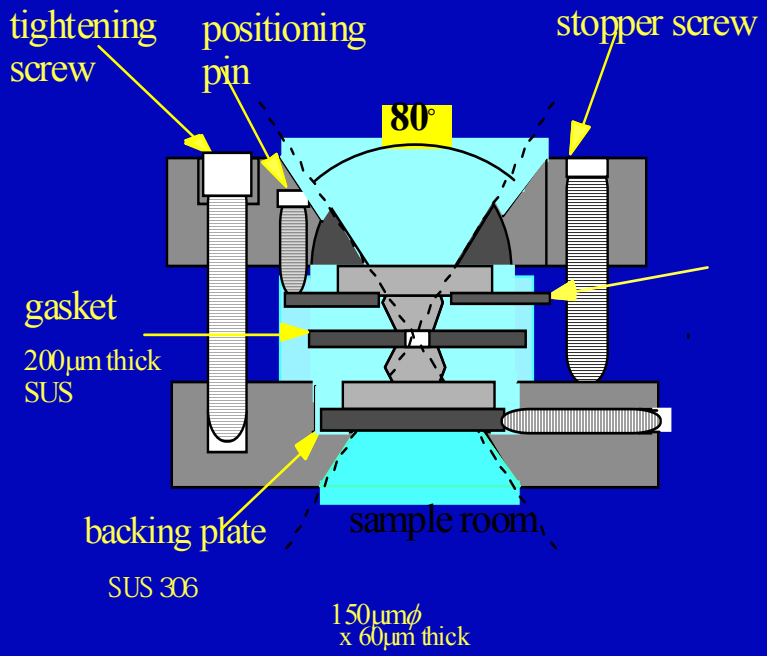

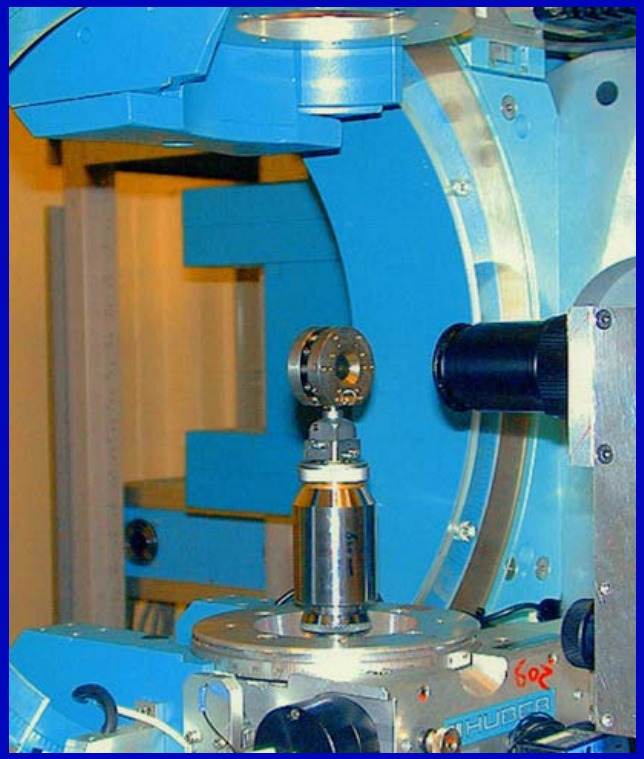

Low temperature experiment

QuickTimeý Ç²
TIFFÅiLZWÅj êLí£ÉvĚçÉOÉâÉÄ
Ç™Ç±ÇÃÉsÉNÉ`ÉÉÇ¾å©ÇÈÇžÇ½Ç…ÇÕïKóvÇ-Ç□ÅB

Lattice constant change

Low-temperature experiment at 1atm

(1) Transition temperature of cubic-to-tetragonal at -110℃

(2) c/a = 1.0035(5) at -170℃.

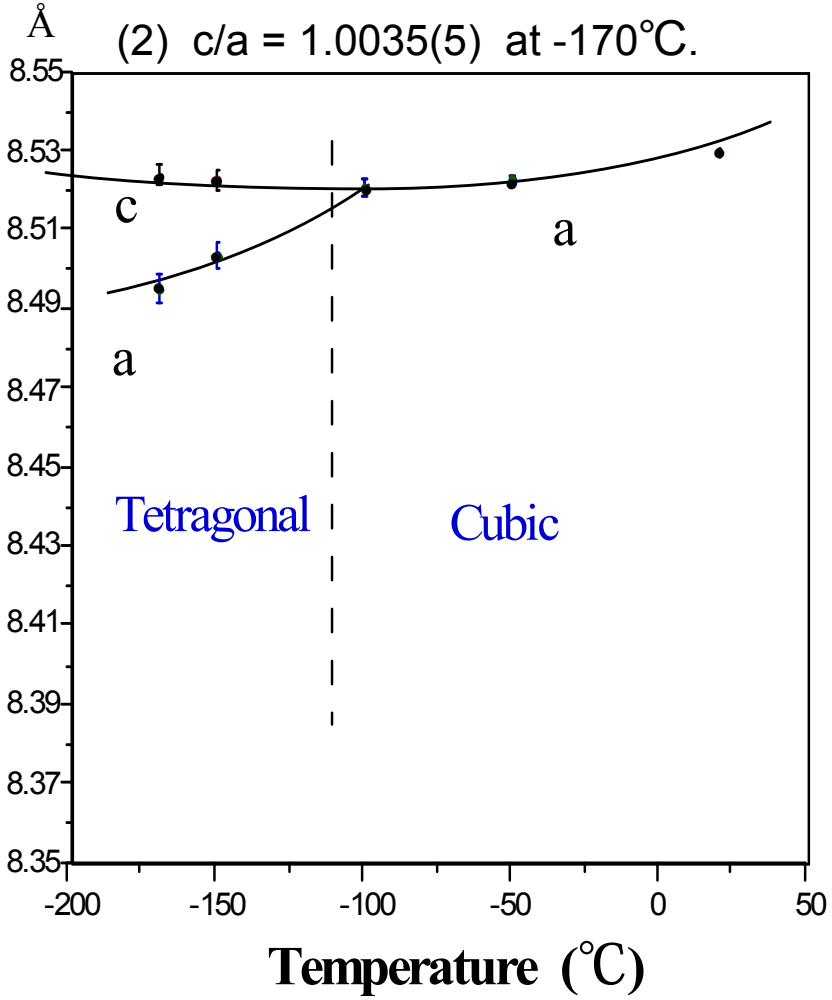

High-pressure experiment at 20℃

(1) Transition pressure of cubic-to-tetragonal at 9 GPa.

(2) c/a = 0.9982(4) at 11.43GPa.

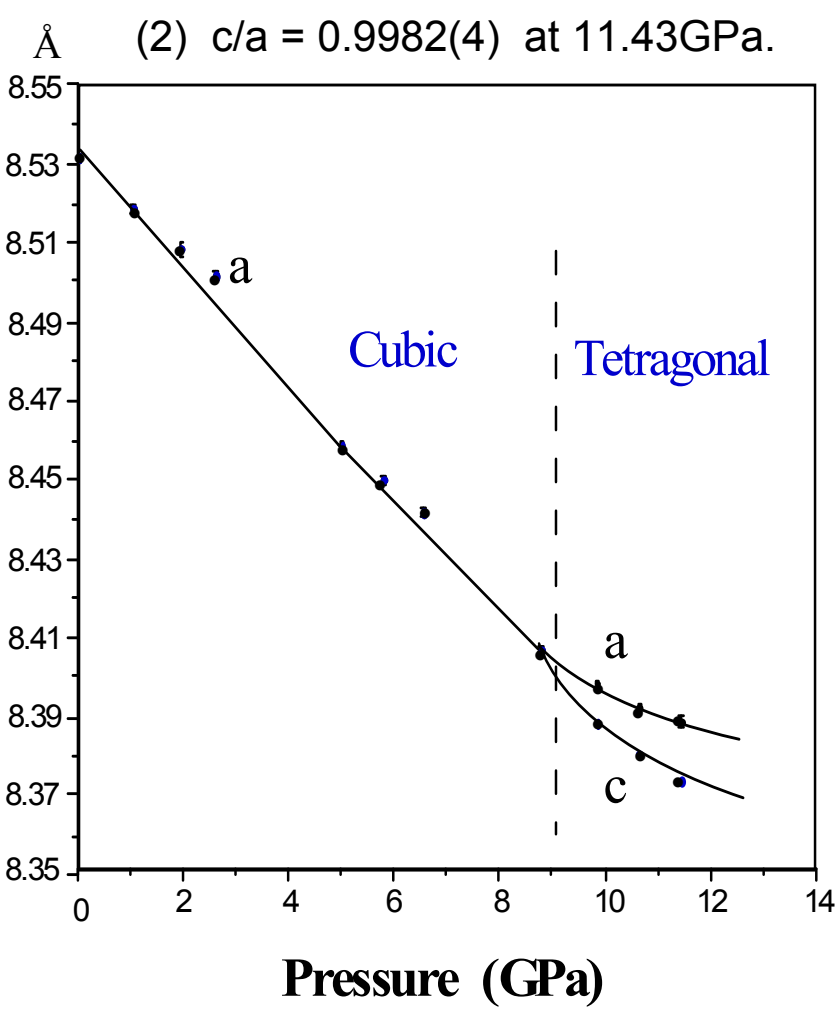

Polyhedral relative volume change

Low-temperature experiment
at 1atm

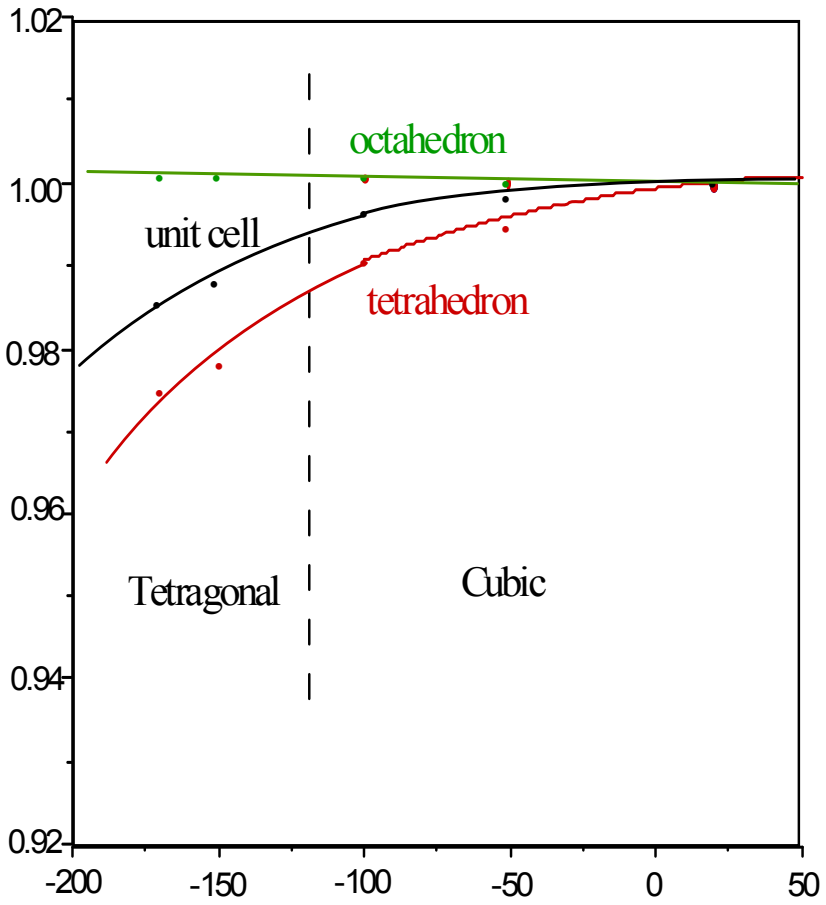

High-pressure experiment
at 20℃

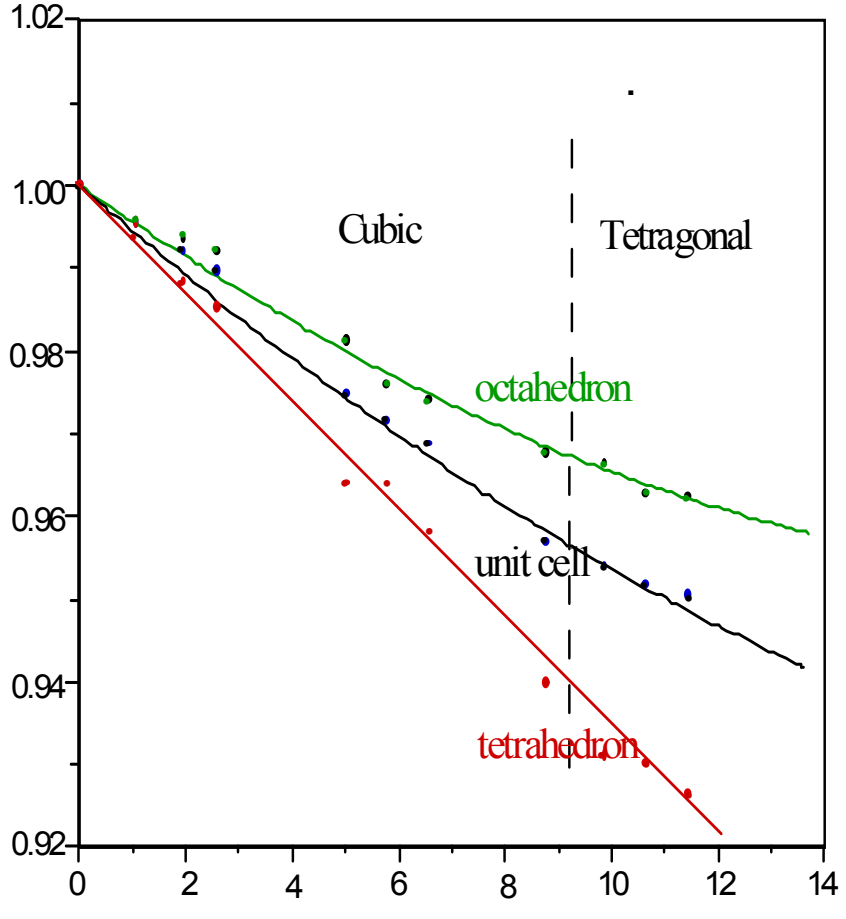

Difference Fourier Map (-170℃)

Residual electron densit

tetragonal phase

contour : 0.2e/Å^3

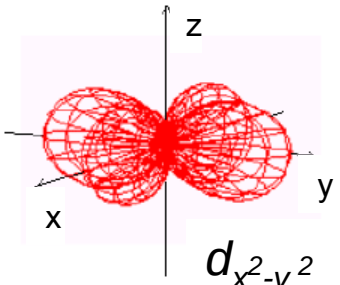

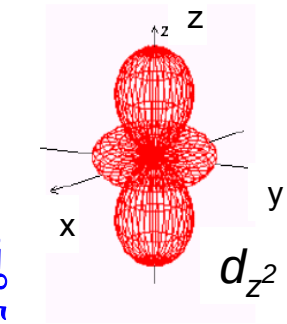

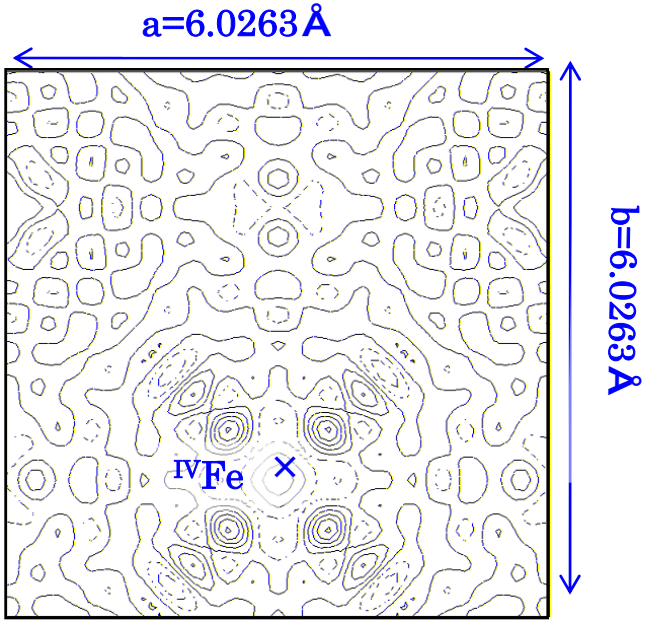

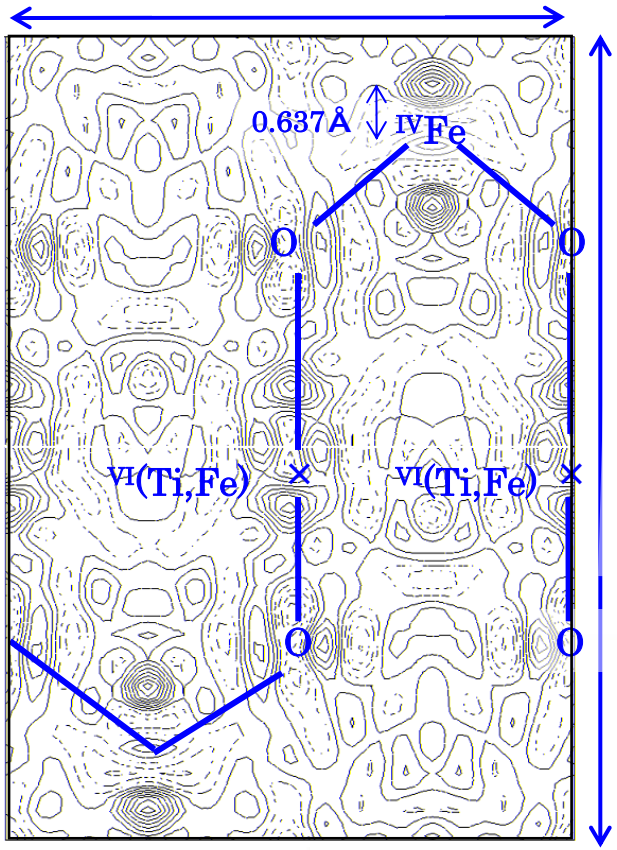

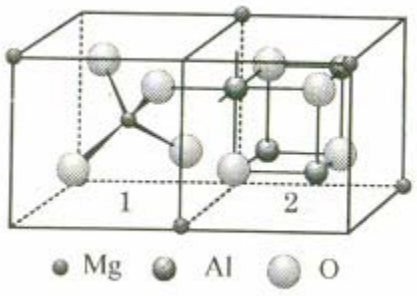

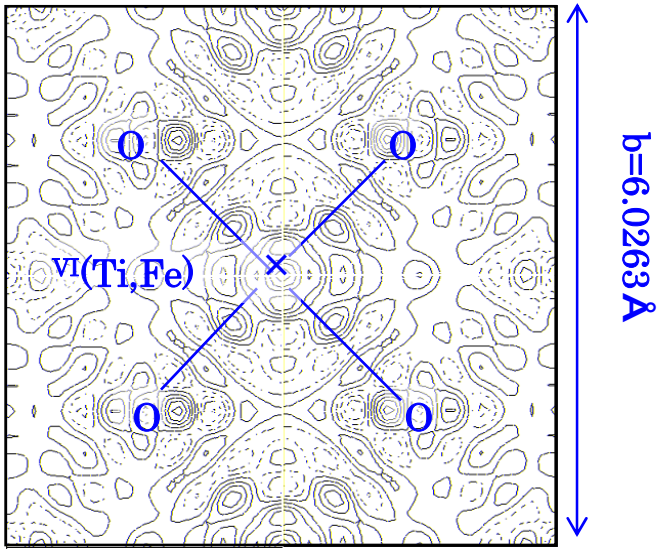

Electron density by Maximum-Entropy Method (MEM)

$$\rho(\vec{r}_i) = \tau(\vec{r}_i)\exp\left[\frac{\lambda F_o}{N}\sum_{\vec{h}}\frac{w(\vec{h})}{\sigma^2(\vec{h})}\left\{F_{obs}(\vec{h}) - F_{cal}(\vec{h})\right\}\exp(-2\pi i\vec{h}\cdot\vec{r}_i)\right]$$

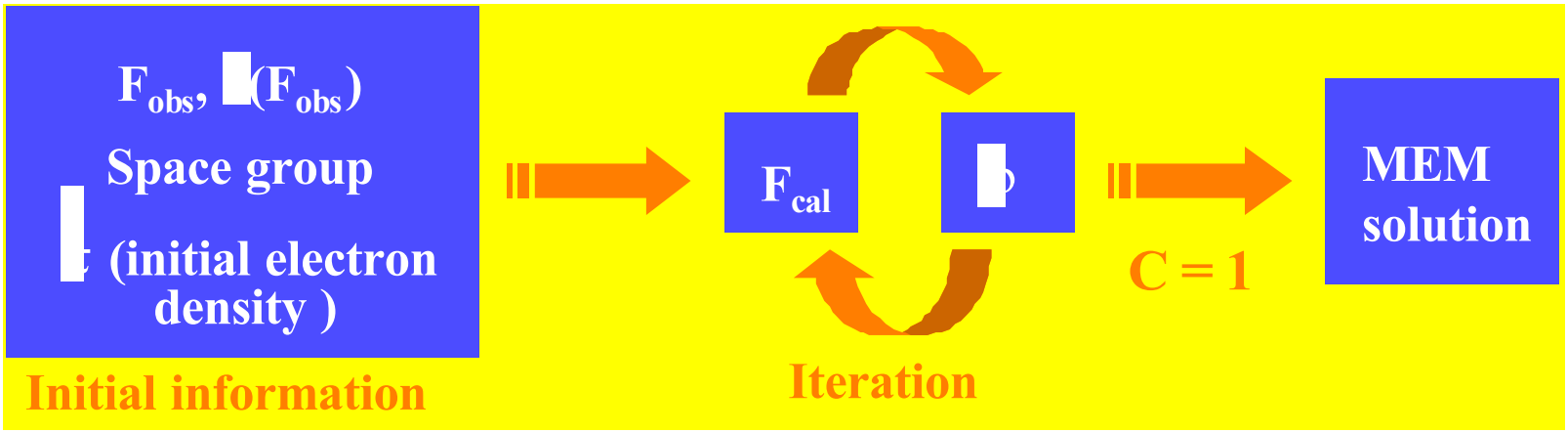

Weighted electron density

$$\rho(\vec{r}_j) = \tau(\vec{r}_j)\exp\left[\frac{\lambda F_0}{N}\sum_{\vec{h}}\frac{w(\vec{h})}{\sigma^2(\vec{h})}\left\{F_{obs}(\vec{h}) - F_{cal}(\vec{h})\right\}\exp(-2\pi i\vec{h}\cdot\vec{r}_j)\right]$$

$w(\vec{h})$: weight

(1) $w(\vec{h}) = 1$ (2) $w(\vec{h}) = F_{obs}(\vec{h})^n \quad n = \frac{1}{2}, 1, 2$ (3) $w(\vec{h}) = \left(\frac{\sin\theta}{\lambda}\right)^{-n} \quad n = \frac{1}{2}, 1, 2$

$\sigma(\vec{h})$: estimated error : $\sigma(\vec{h}) = a \times \left(\frac{\sin\theta}{\lambda}\right) + b$

MEM electron density map on to (110)

Ambient condition

Low temperature

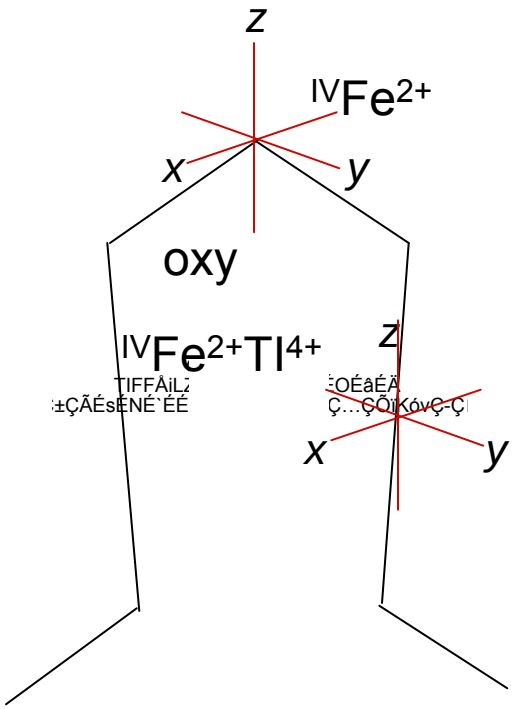

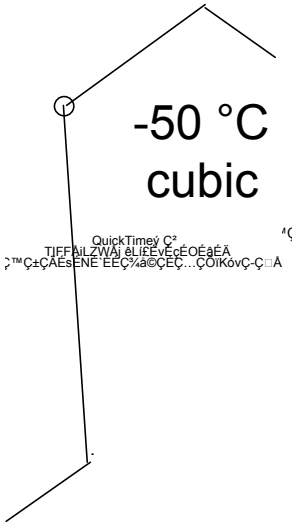

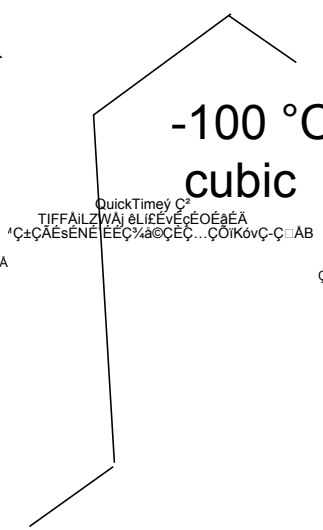

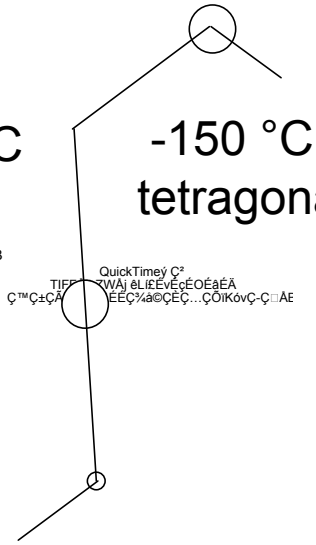

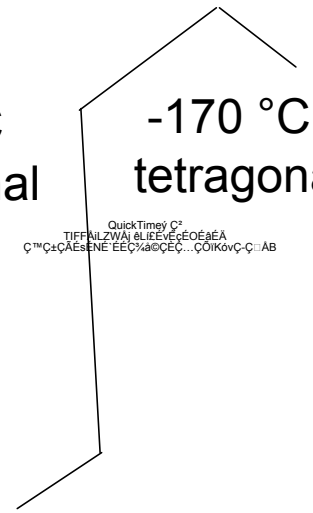

High pressure

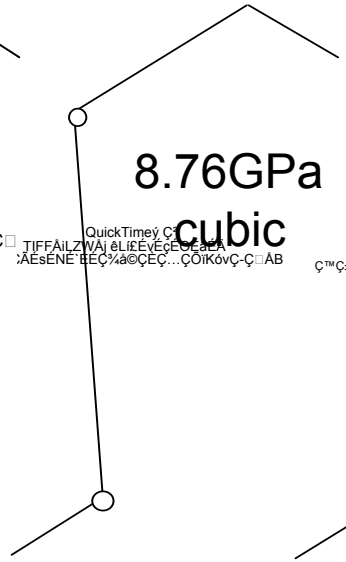

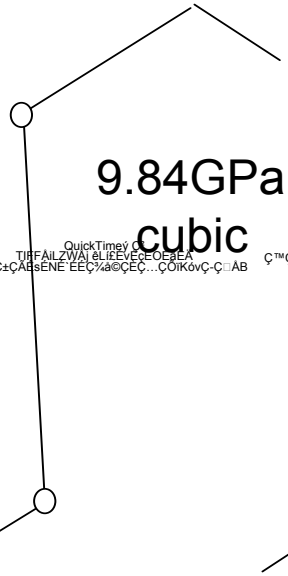

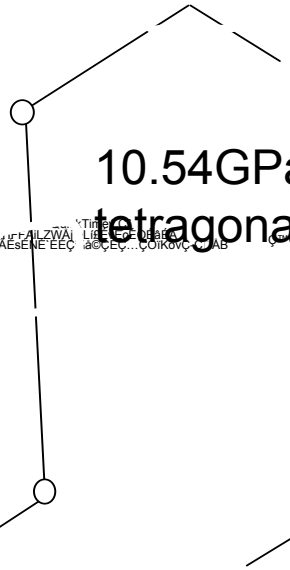

Spinel structure
asymmetric unit

MEM electron density map on to (110)

Ambient condition

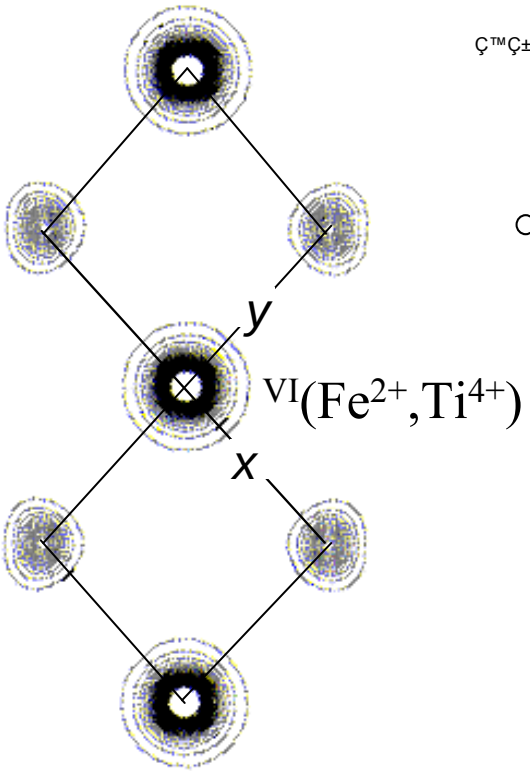

Low temperature

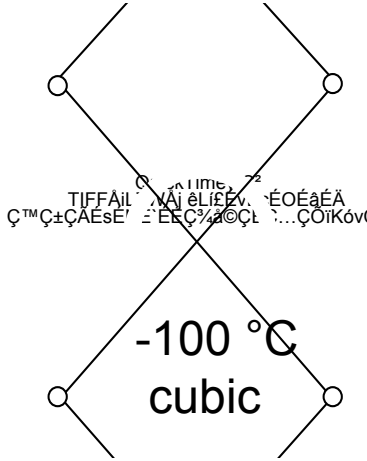

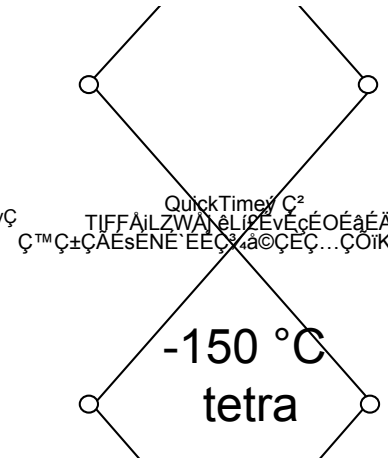

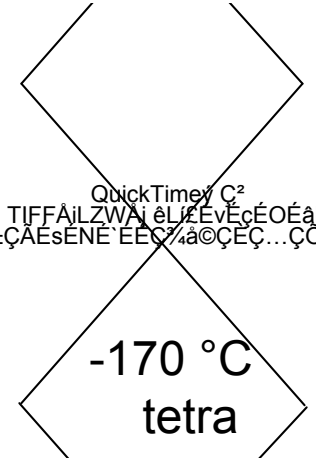

High pressure

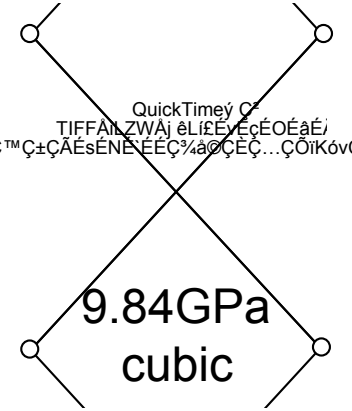

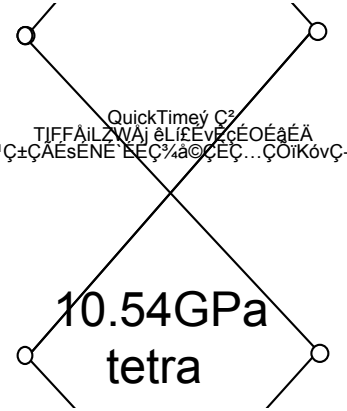

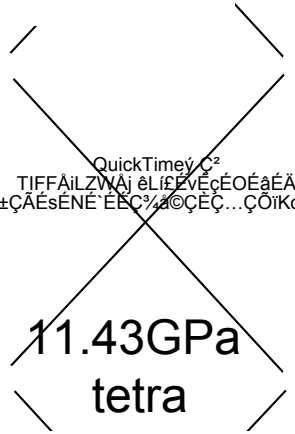

∠O-Fe-O of $Fe^{2+}O_4$ tetrahedral bond angle

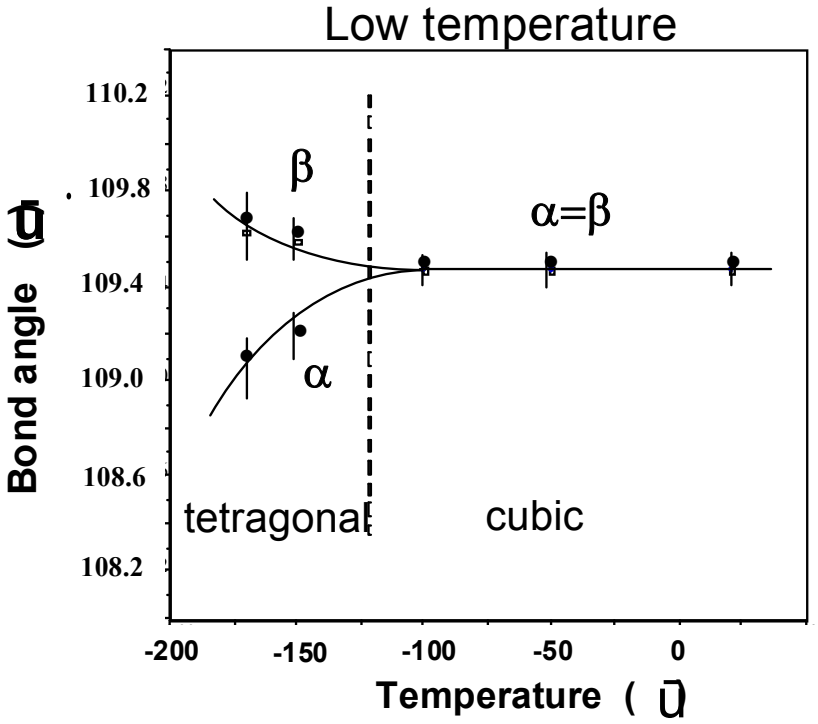

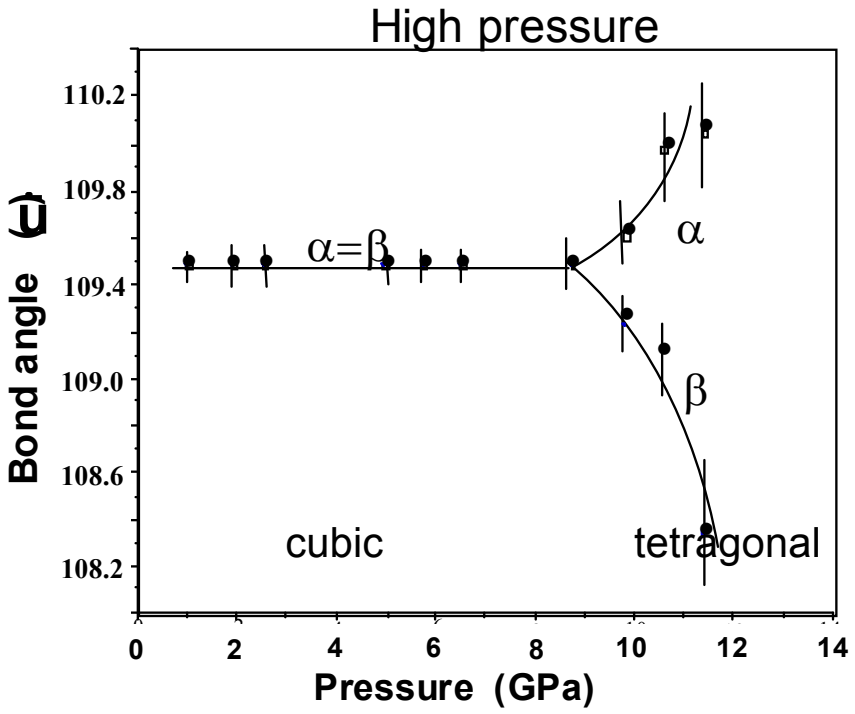

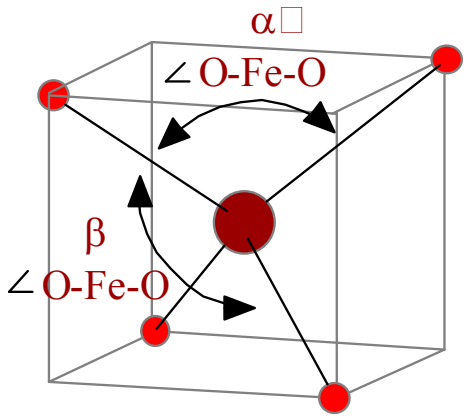

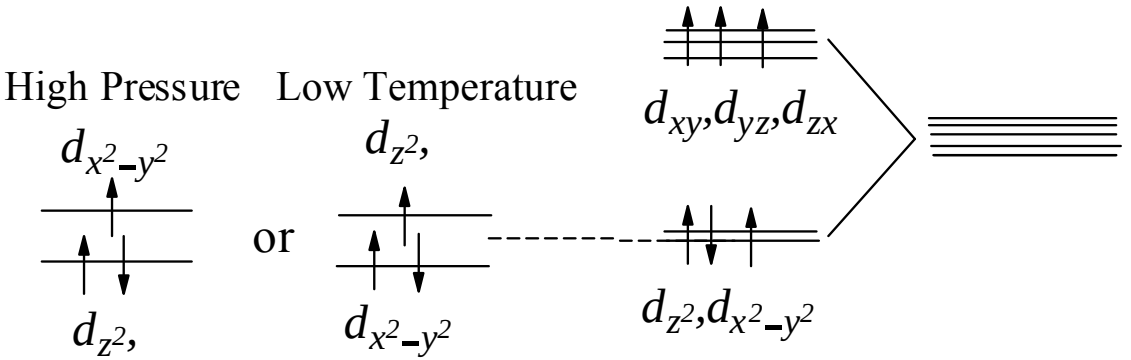

tetragonal ($\bar{4}$2m)
tetrahedral configuration

cubic ($\bar{4}$3m) (m3) (23)
tetrahedral configuration

Anisotropy of electric conduction in ilmenite under high pressure

electron hopping by super exchange

Sample :

$FeTiO_3$ ilmenite

$R\bar{3}$ z= 6 hexagonal a= 5.0881Å c= 14.9 10Å

Electric conduction of $FeTiO_3$ ilmenite

QuickTimeý Ç²
TIFFÅiLZWÅj êLíŁÉvÉçÉOÉâÉÄ
Ç™Ç±ÇÃÉsÉNÉ`ÉÉÇ¾å©ÇÈÇžÇ½Ç…ÇÕïKóvÇ-Ç□ÅB

QuickTimeý Ç²
TIFFÅiLZWÅj êLíŁÉvÉçÉOÉâÉÄ
Ç™Ç±ÇÃÉsÉNÉ`ÉÉÇ¾å©ÇÈÇžÇ½Ç…ÇÕïKóvÇ-Ç□ÅB

QuickTimeý Ç²
TIFFÅiLZWÅj êLíŁÉvÉçÉOÉâÉÄ
Ç™Ç±ÇÃÉsÉNÉ`ÉÉÇ¾å©ÇÈÇžÇ½Ç…ÇÕïKóvÇ-Ç□ÅB

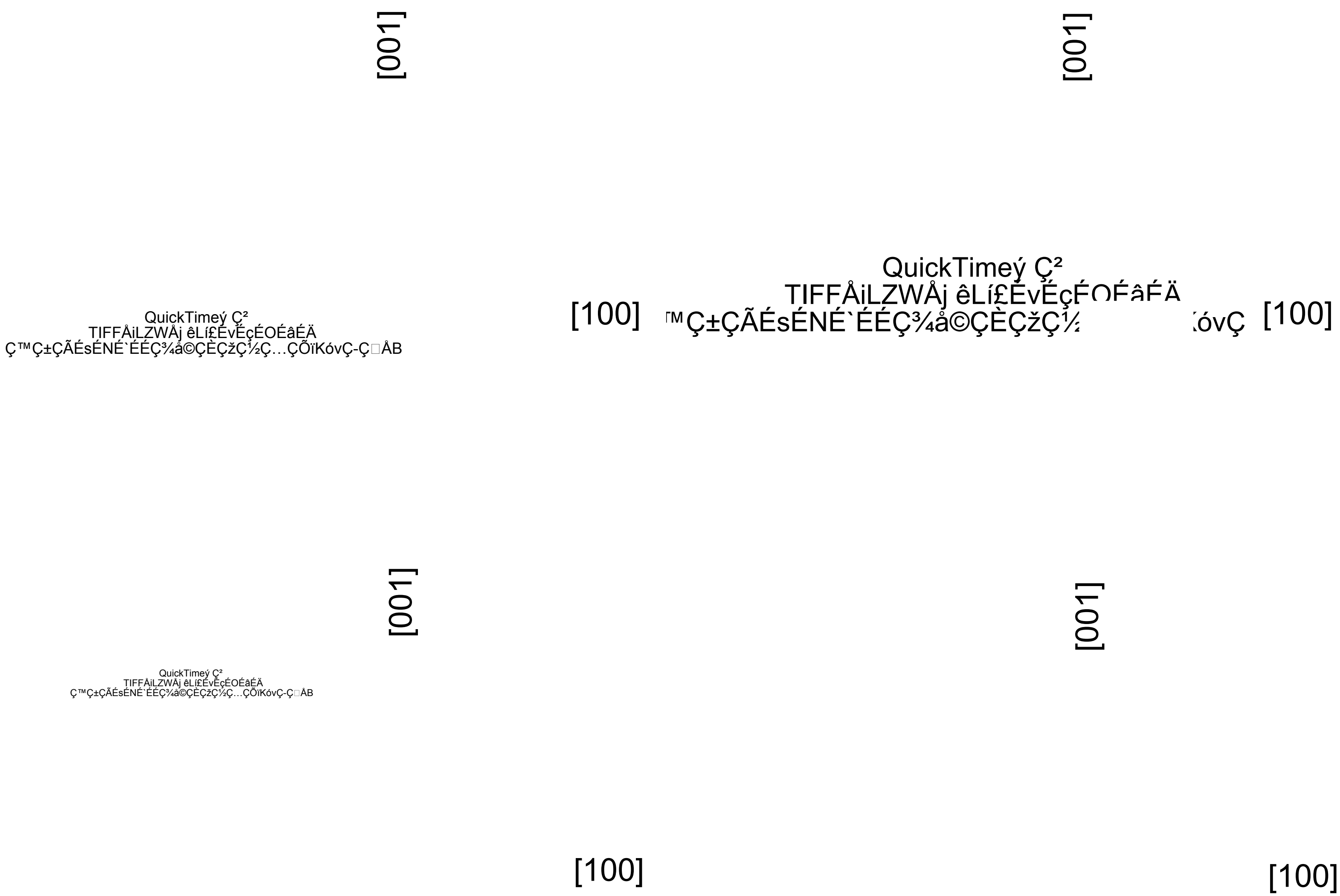
[001]
[100]
[001]
[100]
[001]
[100]
[001]
[100]

Radial distribution of electron density distribution

Electron density (eÅ^{-3})

QuickTimeý Ç²
TIFFÅiLZWÅj êLí£ËvÉçÉOÉâÉÄ
Ç™Ç±ÇÃÉsÉNÉ`ÉÉÇ¾å©ÇÈÇžÇ½Ç…ÇÕïKóvÇ-Ç□ÅB

Z-coordinate

[001]

[001]

[110]

QuickTimeý Ç²
TIFFÅiLZWÅj êLí£ËvÉçÉOÉâÉÄ
Ç™Ç±ÇÃÉsÉNÉ`ÉÉÇ¾å©ÇÈÇžÇ½Ç…ÇÕïKóvÇ-Ç□ÅB

[110]

[001]

[001]

[110]

[110]

Conclusion

1. $Mn_2O_{3c}$of cubic bixbyite structure is transformed to post-perovskite structure over 21GPa and Jahn-Teller effect in the structure is suppressed under pressure.
2. After laser heating 1400 C, the post-perovskite structure is changed monoclinic Gd2O3 structure.
3. X-ray emission spectrum analysis proved these transitions are not induced from high-low spin transition or charge displopornation.
4. From MEM electron density distribution analysis, the Jahn-Teller distortion caused by $^{IV}Fe^{2+}$ of Fe_2TiO_4 ulvöspinel is different between at high pressure and low temperature. Electron configurations in e-orbit and t_2 are different in these conditions.
5. Anisotropy of Electric conduction in $FeTiO_3$ was confirmed with increasing pressure.

QuickTimeý Ç²
TIFFÅiLZWÅj êLí£ÉvÉçÉOÉâÉÄ
Ç™Ç±ÇÃÉsÉNÉ`ÉÉÇ¾å©ÇÈÇžÇ½Ç…ÇÕïKóvÇ-Ç□ÅB

QuickTimeý Ç²
TIFFÅiLZWÅj êLí£ÉvÉçÉOÉâÉÄ
Ç™Ç±ÇÃÉsÉNÉ`ÉÉÇ¾å©ÇÈÇžÇ½Ç…ÇÕïKóvÇ-Ç□ÅB

Electron spin configuration of transition elements

in cubic symmetry

8-fold coordination
hexahedron

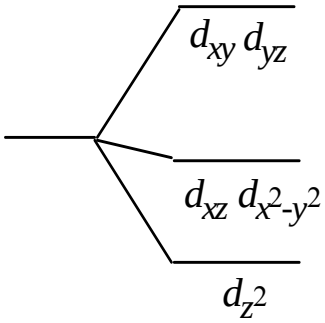

8-fold coordination
antidipiramid

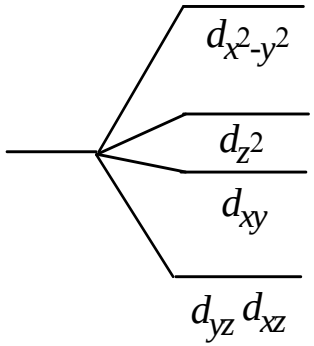

6-fold coordination
octahedron
tetragonal dipiramid

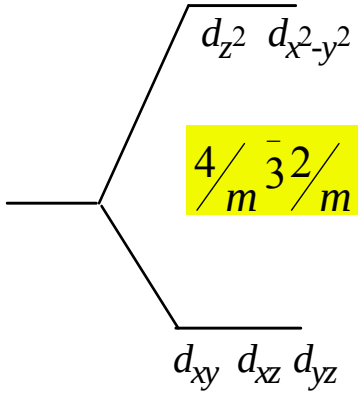

5-fold coordination
trigonal dipiramid

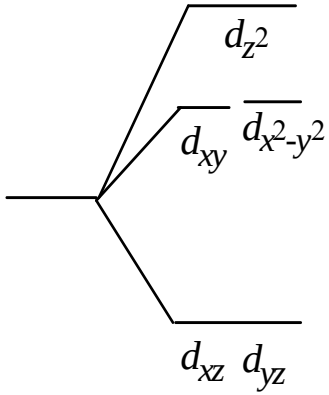

5-fold coordination
rhombohedron

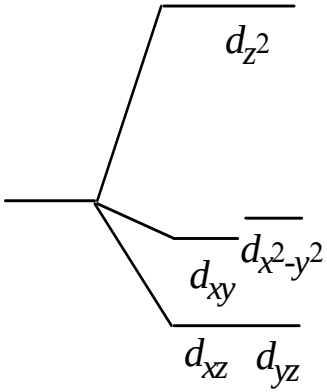

4-fold coordination
tetrahedron

$\bar{4}\,32$

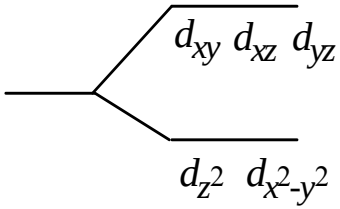

4-fold coordination
coplanar square

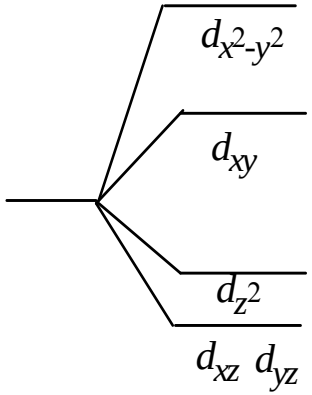

3-fold coordination
coplanar trigon